

Flow of Cortical Activity Underlying a Tactile Decision in Mice

Zengcai V. Guo,^{1,3} Nuo Li,^{1,3} Daniel Huber,^{1,4} Eran Ophir,¹ Diego Gutnisky,¹ Jonathan T. Ting,² Guoping Feng,² and Karel Svoboda^{1,*}

¹Janelia Farm Research Campus, HHMI, Ashburn, VA 20147, USA

²McGovern Institute for Brain Research and Department of Brain and Cognitive Sciences, Massachusetts Institute of Technology, Cambridge, MA 02139, USA

³These authors contributed equally to this work

⁴Present address: Department of Basic Neurosciences, University of Geneva, CH-1211 Geneva, Switzerland

*Correspondence: svobodak@janelia.hhmi.org
<http://dx.doi.org/10.1016/j.neuron.2013.10.020>

SUMMARY

Perceptual decisions involve distributed cortical activity. Does information flow sequentially from one cortical area to another, or do networks of interconnected areas contribute at the same time? Here we delineate when and how activity in specific areas drives a whisker-based decision in mice. A short-term memory component temporally separated tactile “sensation” and “action” (licking). Using optogenetic inhibition (spatial resolution, 2 mm; temporal resolution, 100 ms), we surveyed the neocortex for regions driving behavior during specific behavioral epochs. Barrel cortex was critical for sensation. During the short-term memory, unilateral inhibition of anterior lateral motor cortex biased responses to the ipsilateral side. Consistently, barrel cortex showed stimulus-specific activity during sensation, whereas motor cortex showed choice-specific preparatory activity and movement-related activity, consistent with roles in motor planning and movement. These results suggest serial information flow from sensory to motor areas during perceptual decision making.

INTRODUCTION

Perceptual decisions involve multiple, spatially distributed cortical areas (Felleman and Van Essen, 1991; Hernández et al., 2010). Romo and colleagues recorded neuronal correlates of sensation, memory, and action in primates during passive tactile decision tasks. Their findings suggest a hierarchically organized cortical system, in which sensory information in primary somatosensory cortex (Zainos et al., 1997) is gradually (Hernández et al., 2010) transformed into choice in frontal cortical areas (de Lafuente and Romo, 2005) (reviewed in Romo and de Lafuente, 2013). Serial information flow has also been observed in visual perceptual decision tasks in primates (Bisley et al., 2001; Gold and Shadlen, 2002; Seidemann et al., 1998). Relating neuronal signals to behavior requires rapid and reversible (within a trial

epoch) silencing of neuronal activity during behavior. Pharmacological silencing (Hikosaka and Wurtz, 1985) and cooling (Long and Fee, 2008; Ponce et al., 2008) are too slow to reveal the involvement of individual brain areas during specific behavioral epochs. Electrical microstimulation has the requisite temporal resolution (Bisley et al., 2001; de Lafuente and Romo, 2005; Seidemann et al., 1998), but all of these methods have low throughput, prohibiting comprehensive surveys of brain regions contributing to behavior.

The mouse is a genetically tractable organism (Luo et al., 2008; O'Connor et al., 2009), providing access to defined cell types for transgene expression. Its lissencephalic macrostructure allows access to a large fraction of the brain for functional analysis. The mouse is therefore a powerful model to examine the circuit mechanisms underlying behavior. Progress will require quantitative perceptual decision tasks and establishing causal relationships between cortical activity in specific brain regions and behavior. The flow of information through interconnected cortical areas underlying a perceptual decision has not been examined in mice. A key challenge is that decision tasks with the requisite behavioral components are not available.

Here we developed a tactile decision behavior in head-fixed mice to track the flow of information during perceptual decision making. Rodents use their whiskers to navigate tight spaces and explore objects (Knutsen et al., 2006; O'Connor et al., 2010a; Ritt et al., 2008; Voigts et al., 2008). In our task, head-fixed mice measured the location of a pole using their whiskers and reported their choice with licking. In contrast to previous versions (O'Connor et al., 2010a), a delay epoch separates “sensation” and “action.” We used optogenetic silencing to identify the cortical regions involved during any trial epoch.

The vibrissal primary somatosensory cortex (vS1, also called “barrel cortex”) receives whisker-related tactile input via the thalamus (Koralek et al., 1988; Lu and Lin, 1993; Petreanu et al., 2009; Woolsey and Van der Loos, 1970). vS1 is heavily connected with thalamic and other cortical areas via long-range connections (Hoffer et al., 2005; Hooks et al., 2013; Mao et al., 2011). The vast majority of cortical areas remain unstudied in the context of tactile discrimination.

Inactivating vS1 caused deficits in object location discrimination (Hutson and Masterton, 1986; O'Connor et al., 2010a, 2013), mainly during sensation. Unilateral inactivation of a frontal

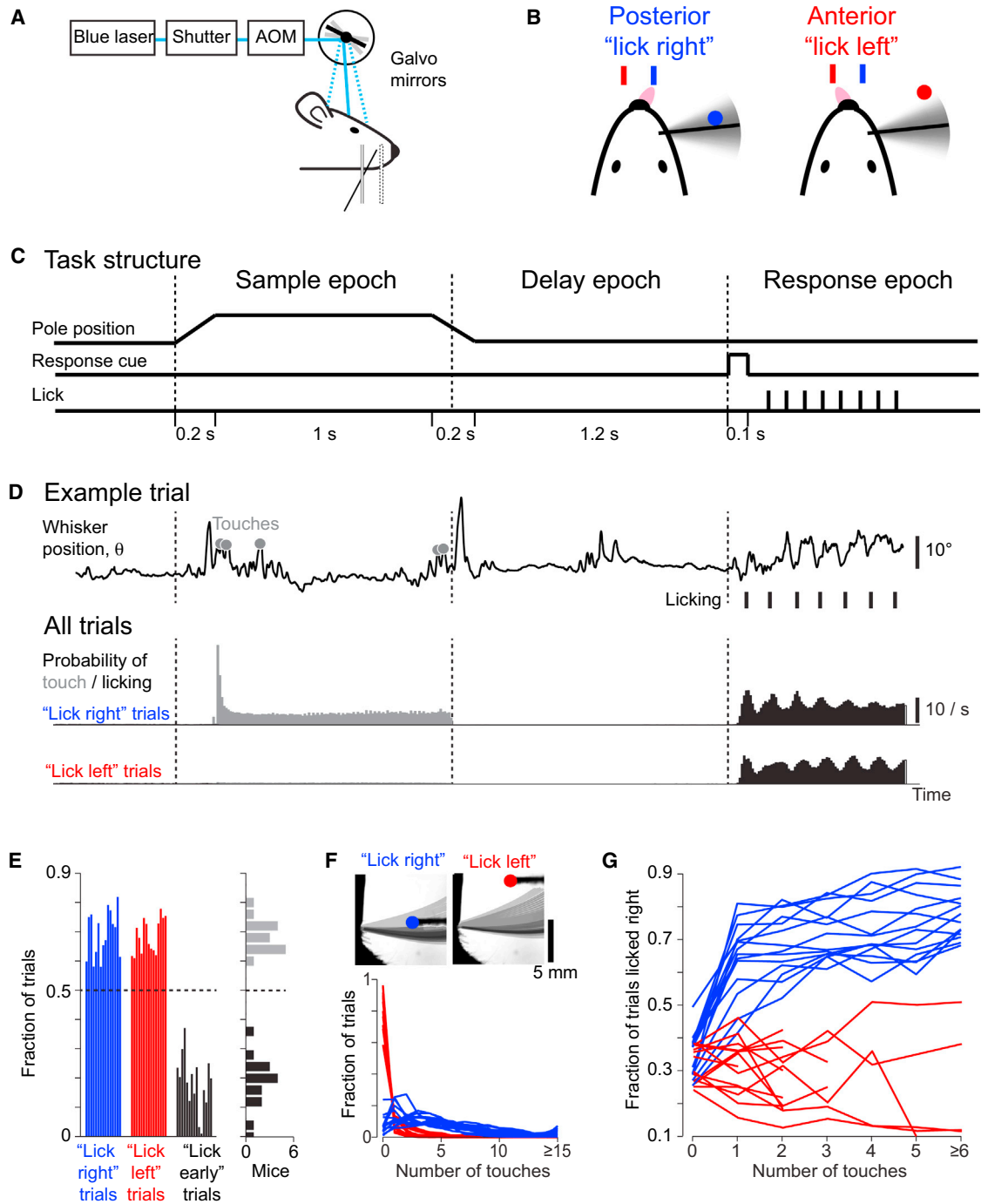


Figure 1. Object Location Discrimination Task with a Delay Epoch

(A) Head-fixed mouse performing object location discrimination under optogenetic perturbation.

(B) A mouse producing "lick right" and "lick left" responses based on pole location.

(C) Task structure. The pole was within reach during the sample epoch. Mice responded with licking after an auditory response cue.

(D) Behavioral data. Top: one example trial. Whisker position (azimuthal angle, θ) for a representative "lick right" trial is shown. Touches, gray circles; licks, black ticks. Middle: summary data for "lick right" trials in eight mice. Probability of touch, gray; licking, black (10 ms time bin). Bottom: same as middle for "lick left" trials.

(E) Behavioral performance across mice. Left: fraction correct "lick right" (blue), "lick left" (red), and "lick early" (black) trials. Each bar corresponds to one mouse ($n = 15$). Right: histogram of performance (gray) and fraction of "lick early" trials (black) across individual mice.

(legend continued on next page)

cortical area (anterior lateral motor cortex [ALM]) during the delay epoch, preceding the motor response, biased the upcoming choice in the ipsilateral direction. Neurons in vS1 showed stimulus-specific activity during the sample epoch (Curtis and Kleinfeld, 2009; O'Connor et al., 2010b; von Heimendahl et al., 2007). Neurons in ALM showed choice-specific preparatory activity and movement-related activity, consistent with roles in driving the response. Our results are consistent with serial information flow, in which information is passed from sensory areas to motor areas during perceptual decision making.

RESULTS

Object Location Discrimination with a Short-Term Memory Epoch

The behavioral task (Figure 1A) was adapted from a lick/no-lick object location discrimination task (O'Connor et al., 2010a) with two modifications: first, mice indicated their choice by symmetrically (Sanders and Kepecs, 2012; Schwarz et al., 2010) licking one of two lickports ("lick left/lick right"); second, mice withheld their response during a delay epoch. The symmetric response ensured that the expectation of reward is independent of choice, minimizing bias toward one of the two responses. In each trial, a vertical pole was presented in one of two positions (anterior or posterior). The mouse was trained to locate the pole with a single whisker (the C2 whisker) and report the perceived pole position by licking (Figure 1B). The standard contingency was: posterior → lick right and anterior → lick left (the contingency was reversed for the experiments of Figure 5). The task was divided into sample, delay, and response epochs, thus separating "sensation" and "action" (Figure 1C) (Tanji and Evarts, 1976). At the beginning of the sample epoch, the pole moved quickly (0.2 s) into reach of the C2 whisker, whereupon the mouse whisked to touch the pole (Figures 1C and 1D). The pole was present during the sample epoch (1.3 s), which terminated when the pole moved out of reach. After the sample epoch was the delay epoch (1.3 s), during which the mouse withheld the response (licking) while remembering its behavioral choice. An auditory cue (0.1 s) signaled the beginning of the response epoch and mice initiated licking (Figure 1D). Premature licking, during the sample or delay epochs, triggered an alarm sound and a brief timeout ("lick early" trials, Figure 1E).

We trained a total of 22 mice in the object location discrimination task (Table 1; fraction correct, $69\% \pm 5\%$, mean \pm SD; Figures 1E and S1A available online). Mice achieved criterion performance (70% correct) within 3 weeks (Figure S1B) with little bias between "lick right" and "lick left" trials (Figure S1C). Mice suppressed licking until the response epoch on a majority of the trials. "Lick early" trials ($18\% \pm 9\%$, mean \pm SD, Figures 1E and S1D) were excluded from our analyses. Rhythmic licking (7.6 ± 0.46 Hz, mean \pm SD; Figure 1D) began immediately after the auditory cue (median reaction time after cue onset, 80.2 ± 10.5 ms, mean \pm SD).

High-speed measurements of whisker movements (see Experimental Procedures; Figure 1F) (Clack et al., 2012; O'Connor et al., 2010a) revealed that the C2 whisker scanned across the posterior pole position (Figure 1F) (O'Connor et al., 2010a). Mice made significantly more touches in posterior trials (4.9 ± 1.2 contacts, mean \pm SD) than in anterior trials (0.4 ± 0.4 contacts, mean \pm SD, $p < 0.001$, t test). Mice thus solved the task using a highly asymmetric whisking strategy. The preference for one pole position over the other ("exploration bias") (Figure S5B) was much higher than in previous experiments without delay epoch (O'Connor et al., 2010a, 2013). This extreme bias suggests that mice solve the task by detecting the pole in the posterior position and ignore the pole in the anterior position. The majority of the touches occurred at the beginning of the sample epoch (Figure 1D). Mice used touch to solve the task: first, "lick right" response probability increased with larger numbers of touches per trial (Figure 1G); second, mice were unable to perform the task after the C2 whisker was trimmed (Figure S1E). Head-fixed mice can perform object location discrimination with a single whisker and hold the decision in memory for a delay epoch.

Inactivating Cortical Activity

To probe the role of specific brain areas, we inactivated small volumes of cortical tissue by photostimulating channelrhodopsin-2 (ChR2) in GABAergic interneurons (VGAT-ChR2-EYFP) (Zhao et al., 2011) (Figure S2). Since GABAergic interneurons have dense local axonal arbors (Helmstaedter et al., 2009), this approach is expected to produce potent and local inhibition (Figure 2A).

We characterized "photoinhibition" in awake mice (Figure S3; see Experimental Procedures). A laser beam (wavelength, 473 nm; Figure S4A) was focused onto the surface of the brain (Figure 1A). Extracellular recordings were made in vS1 close to the center of the laser ($n = 133$ isolated single units, see Experimental Procedures; Figure S3). The distribution of spike widths was bimodal (Figures 2B and 2C). Fast-spiking (FS) neurons with narrow spikes were probably parvalbumin-positive interneurons (Kawaguchi, 1993; McCormick et al., 1985), and these neurons were activated by photostimulation, on average (Figures 2B and 2D). Neurons with wide spikes probably were mostly pyramidal neurons (putative pyramidal [ppyr] neurons) and were inhibited by photostimulation (Figures 2B and 2D). To quantify inhibition of the ppyr neurons (see Experimental Procedures, $n = 106$), we normalized the firing rate during photostimulation to the baseline firing rate ("normalized spike rate," see Experimental Procedures; range of baseline firing rates, 0.01–28.8 spikes/s; mean firing rate, 5.5 spikes/s). Near the center of the photostimulus (< 1 mm from the laser center), activity of the ppyr neurons was reduced over a wide range of power levels (Figure 2E). At moderate laser powers (1.5 mW; $87\% \pm 3\%$ activity reduction, mean \pm SEM; 83/106 significantly inhibited, $p < 0.05$, t test), photoinhibition was localized to a region with radius

(F) Top: whisker density for representative "lick right" and "lick left" trials (overlaid whisker images). Bottom: distribution of the number of touches in "lick right" and "lick left" trials. Each line corresponds to one mouse ($n = 14$).

(G) The fraction of "lick right" responses as a function of number of touches for "lick right" (blue) and "lick left" (red) trials ($n = 14$). One mouse from (E) was excluded because there were not enough trials to sort by the number of touches (Table 1). See also Figure S1.

Table 1. Mice Appearing in This Paper

Mouse	Number of Sessions ^a	Number of Trials	Number of Recording Sessions	Number of Recorded Neurons	Experiment Types	Figures
JF140689 (female)	12	4,905	3	23	vS1 spatial photoinhibition, vS1 sample versus delay photoinhibition, S1 recording	1D–1G, 3C, 3E, 4C, 5B, 6C, 6D, S4I, and S7
JF138070 (male)	17	6,903	0	0	vS1 spatial photoinhibition, vS1 sample versus delay photoinhibition	1D–1G, 3C, 3E, 4C, 5B, S4I, and S7
JF138072 (male)	9	3,191	1	3	vS1 spatial photoinhibition, vS1 sample versus delay photoinhibition, vS1 recording	1D–1G, 3C, 3E, 4C, 5B, 6C, 6D, S4I, and S7
JF147593 (male)	9	3,450	0	0	vS1 sample versus delay photoinhibition	1D, 1E, 3C, 4C, and 5B
JF147595 (male)	18	6,534	2	17	vS1 laser power versus photoinhibition, vS1 sample versus delay photoinhibition, ALM sample versus delay photoinhibition, left ALM recording	1D–1G, 3C, 3D, 4C, 4D, 5B, 7C–7G, S4I, and S7
JF160925 (male)	24	9,909	1	15	vS1 laser power versus photoinhibition, vS1 spatial photoinhibition, vS1 sample versus delay photoinhibition, S1 recording	1D–1G, 3C–3E, 4C, 5B, 6C, 6D, S4I, and S7
JF163936 (male)	29	12,645	3	13	vS1 laser power versus photoinhibition, vS1 spatial photoinhibition, vS1 sample versus delay photoinhibition, vS1 recording	1D–1G, 3C–3E, 4C, 5B, 6C, 6D, S4I, and S7
JF163938 (male)	35	14,564	5	61	vS1 laser power versus photoinhibition, neocortex spatial photoinhibition, vS1 sample versus delay photoinhibition, ALM sample versus delay photoinhibition, left ALM recording, right ALM recording	1D–1G, 3C, 3D, 4B–4E, 5B, 7C–7G, S4I, S6A, S6B, and S7
JF166185 (female)	29	11,260	3	17	vS1 laser power versus photoinhibition, vS1 spatial photoinhibition, vS1 sample versus delay photoinhibition, vS1 recording	1D–1G, 3C–3E, 4C, 5B, 6C, 6D, S4I, and S7
JF147596 (male)	57	22,590	0	0	Neocortex spatial photoinhibition	1D–1G, 3C, 4B, 5B, S1, S6A, and S6B
JF147594 (male)	85	30,990	5	39	vS1 laser power versus photoinhibition, vS1 sample versus delay photoinhibition, ALM sample versus delay photoinhibition, neocortex spatial photoinhibition, vS1 recording, left ALM recording	1D–1G, 3C, 3D, 4B–4E, 5B, 6C, 6D, 7C–7G, S1, S4I, S6A, S6B, and S7
JF147599 (female)	34	10,099	0	0	Neocortex spatial photoinhibition, vS1 laser power versus photoinhibition, vS1 sample versus delay photoinhibition	1D–1G, 3C, 3D, 4B, 4C, 5B, S1, S6A, and S6B
JF166182 (male)	69	36,055	5	31	vS1 laser power versus photoinhibition, vS1 sample versus delay photoinhibition, vS1 spatial mapping, ALM sample versus delay photoinhibition, neocortex spatial photoinhibition, vS1 recording, left ALM recording	1D–1G, 3C–3E, 4B–4E, 5B, 6C, 6D, 7C–7G, S4I, S6A, S6B, and S7
JF167783 (male)	26	12,763	5	41	vS1 laser power versus photoinhibition, vS1 sample versus delay photoinhibition, vS1 spatial photoinhibition, ALM sample versus delay photoinhibition, vS1 recording, left ALM recording	1D–1G, 3C–3E, 4C–4E, 5B, 6C, 6D, 7C–7G, S4I, and S7
JF167784 (male)	39	21,959	5	41	vS1 laser power versus photoinhibition, vS1 sample versus delay photoinhibition, vS1 spatial photoinhibition, ALM sample versus delay photoinhibition, vS1 recording, left ALM recording	1D–1G, 3C–3E, 4C–4E, 5B, 6C, 6D, 7C–7G, S4I, and S7
JF190962 (male)	29	11,744	0	0	Neocortex spatial photoinhibition	4B, S6A, and S6B
JF173436 (male)	35	13,044	0	0	vS1 reverse contingency, ALM reverse contingency, targeted photoinhibition experiments	5D and S6C–S6H
JF173437 (male)	34	11,918	0	0	vS1 reverse contingency, ALM reverse contingency, targeted photoinhibition experiments	5D and S6C–S6H
JF185608 (male)	16	6,036	0	0	vS1 reverse contingency, ALM reverse contingency, targeted photoinhibition experiments	5D and S6C–S6H

(Continued on next page)

Table 1. Continued

Mouse	Number of Sessions ^a	Number of Trials	Number of Recording Sessions	Number of Recorded Neurons	Experiment Types	Figures
JF155551 (male)	6	2,172	0	0	Wild type, photostimulation, C2 whisker trimming	S1E and S5
JF155552 (male)	4	1,137	0	0	Wild type, photostimulation, C2 whisker trimming	S1E and S5
JF155553 (male)	4	1,013	0	0	Wild type, photostimulation, C2 whisker trimming	S1E and S5
JF152330 (male)	–	–	3	20	vS1 recording, nonbehaving	2, S3, and S4
JF159681 (male)	–	–	1	4	vS1 recording, nonbehaving	2, S3, and S4
JF159342 (male)	–	–	3	26	vS1 recording, nonbehaving	2, S3, and S4
JF152965 (female)	–	–	4	17	vS1 recording, nonbehaving	2, S3, and S4
JF152142 (male)	–	–	4	28	vS1 recording, nonbehaving	2, S3, and S4
JF152143 (male)	–	–	2	4	vS1 recording, nonbehaving	2, S3, and S4
JF152962 (male)	–	–	2	8	vS1 recording, nonbehaving	2, S3, and S4
JF161464 (male)	–	–	4	31	vS1 recording, nonbehaving	2, S3, and S4
JF175015 (male)	–	–	3	24	striatum recording, nonbehaving	S2
JF175016 (male)	–	–	3	15	striatum recording, nonbehaving	S2
JF211314 (female)	–	–	–	–	Clear-skull cap measurement	S4
JF179413 (female)	–	–	–	–	Clear-skull cap measurement	S4
JF212537 (female)	–	–	–	–	Photobleaching experiment	S4
JF212538 (female)	–	–	–	–	Photobleaching experiment	S4

^aIncluding session in which neuronal recording was carried out during active behavior (column 4).

of approximately 1 mm (radius at half-max, Figure 2F). At higher powers (14 mW), neurons were inhibited further from the center of the photostimulus (Figure 2F). Photoinhibition was nearly uniform across cortical layers (Figure 2G; Figure S4J). ChR2-YFP expression was largely absent in the striatum beneath the cortex and recording experiments confirmed that inhibition directly caused by photostimulation was confined to neocortex (Figure S2). Photoinhibition reached steady state 17.3 ms after photostimulus onset with an offset time of 124 ms (see Experimental Procedures).

Inactivating vS1 during Behavior

Studies using aspiration lesions and pharmacological silencing have implicated vS1 in object localization (Hutson and Masteron, 1986; O'Connor et al., 2010a). We thus photoinhibited cortical activity transiently during the sample epoch in the C2 and surrounding columns (Figures 1 and 3A). We obtained optical access to the neocortex (lateral \pm 4 mm, bregma \pm 3 mm) by outfitting mice with a clear-skull cap (Figure 3B, light transmission, approximately 50%; see Experimental Procedures). During behavior we therefore photostimulated directly through the clear-skull cap.

C2 barrel columns were mapped with intrinsic signal imaging (Figure 3B) (Masino et al., 1993; O'Connor et al., 2010b). Photoinhibition at our standard photostimulation condition (1.5 mW) spanned multiple barrel columns, centered on the C2 column (Figure 3A; 85% reduction in spike rate at laser center; 0.9 mm radius at half-max; approximated from Figures 2E and 2F assuming 50% light attenuation). Photoinhibition in behaving mice was nearly as strong as that observed under nonbehaving condition (Figures 2E and S4;

measured without the clear-skull cap to enable direct comparison between behaving and nonbehaving condition: $p = 0.33$, t test at 1.5 mW; 6 mice, 35 vS1 neurons, see Experimental Procedures).

We inactivated vS1 in 15 mice (Table 1) during behavior. Mice performed a large number of trials per session (422 ± 115 trials, mean \pm SD; Table 1). Photostimuli were applied (Figure 2D) randomly in 25% of the trials. Because mice employed a whisking strategy that appeared to maximize touches for “lick right” trials (corresponding to the posterior pole position) and minimize touches in “lick left” trials (Figure 1F), a neuronal signal coding for touch was probably responsible for detection of the pole in “lick right” trials. A simple prediction is that inactivating vS1 reduces performance in “lick right” trials. Consistent with this hypothesis, photoinhibition decreased performance in “lick right” trials (performance reduction, $29.8\% \pm 9.4\%$, mean \pm SD, $p < 0.001$, two-tailed t test, Figure 3C). This deficit increased as a function of light intensity (Figure 3D), implying a relationship between vS1 activity and pole detection. We observed little effect in performance on “lick left” trials (Figure 3D). The behavioral change was not due to nonspecific effects of photostimulation, since light itself, without the *VGAT-ChR2* transgene, produced no effect (Figure S5A). Photoinhibition did not change whisking (Figures S5C and S5D) or the number of touches (paired t test, $p > 0.05$; Figure S5E), despite a deficit in reporting pole location (Figure S5F). In addition, photoinhibition did not change the fraction of “lick early” trials and “no lick” trials (Figure S5A).

We next measured the spatial resolution of photoinhibition in behaving mice. The behavioral effect decreased rapidly with distance of the laser from C2, vanishing at 1.35 ± 0.6 mm

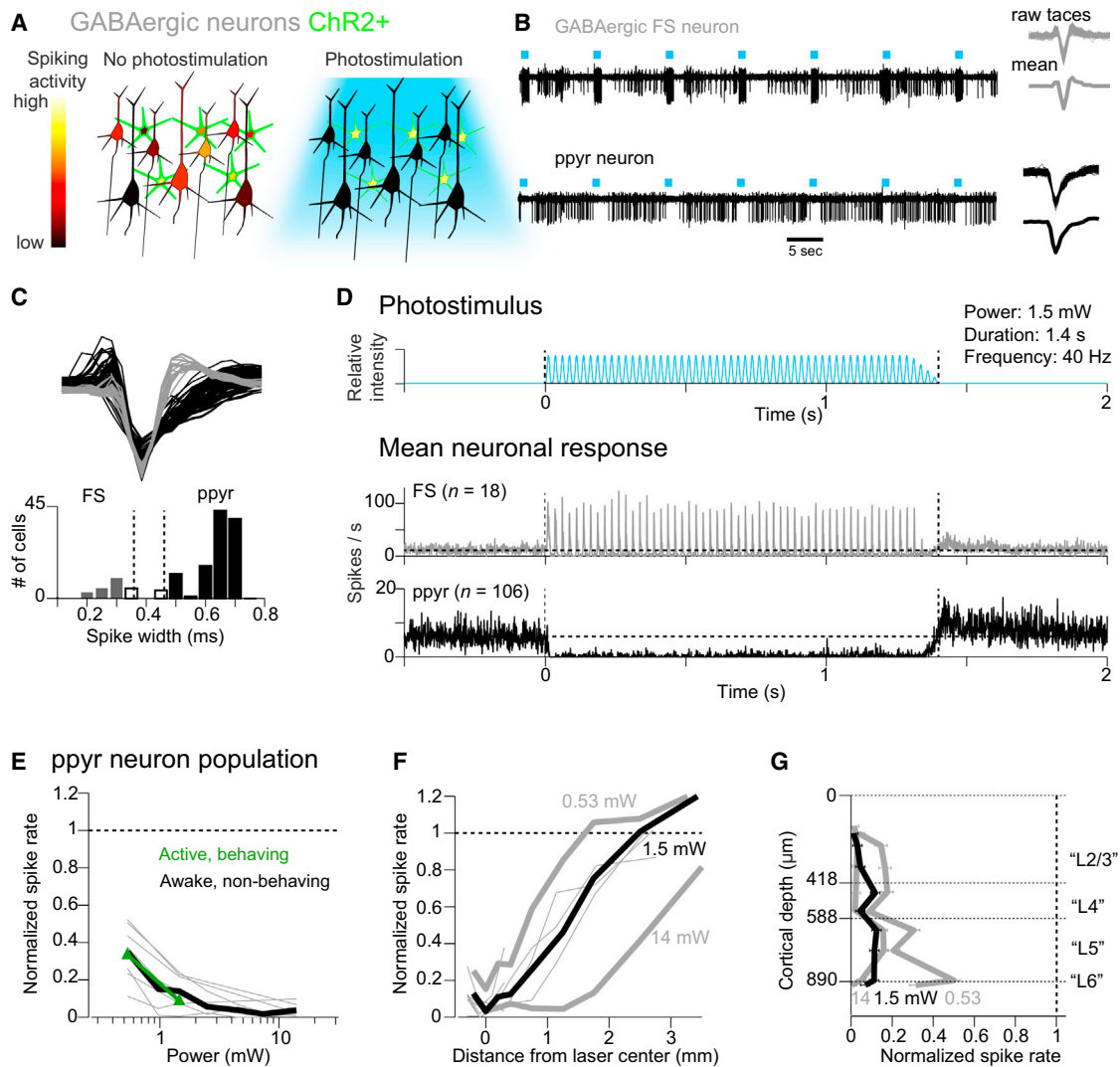


Figure 2. ChR2-Assisted Photoinhibition

(A) Inactivation by photostimulating ChR2-positive GABAergic interneurons (green).
 (B) Silicon probe recordings. Top: a GABAergic fast-spiking (FS) neuron (other units with smaller spike amplitudes were also recorded on this electrode). Bottom: a putative pyramidal (ppyr) neuron. Right: corresponding spike waveforms.
 (C) Spike classification. Top: spike waveforms for FS neurons ($n = 18$; gray) and ppyr neurons ($n = 106$; black). Bottom: histogram of spike durations. Neurons that could not be classified based on spike width were excluded from analysis (white bar, $n = 9$; see [Experimental Procedures](#)).
 (D) Top: the photostimulus. Vertical dotted lines: start and stop of photostimulation. Bottom: mean peristimulus time histogram (PSTH, 1 ms bin) for FS neurons and ppyr neurons recorded under awake, nonbehaving conditions. All neurons <0.25 mm from the laser center were pooled.
 (E) Spike rate as a function of laser power (<1 mm from laser center, all cortical depths). Spike rates were normalized to baseline (dash line, see [Experimental Procedures](#)). Thick black line, mean for awake, nonbehaving condition. Thin gray lines, individual mice (seven mice, 103 ppyr neurons; one mouse with only three ppyr neurons was excluded). Green line, mean for active behaving condition (35 neurons, six mice; error bars reflect SEM over mice).
 (F) Normalized spike rate versus distance from the photostimulus center (all cortical depths). Neurons were pooled across cortical depths. Thin lines, individual mice for the 1.5 mW condition.
 (G) Normalized spike rate versus cortical depth (<0.2 mm from laser center). Recording depths and cortical layers (“L”) are based on histology. Error bars indicate SEM over neurons ($n = 106$). See also [Figures S2, S3, and S4](#).

(mean \pm SEM) from the C2 barrel center ($p > 0.05$, two-tailed t test) ([Figure 3E](#)). The behavioral effect was thus caused by photoinhibition of vS1 and not the surrounding cortical areas. We conclude that touch-evoked activity in vS1 is critical for whisker-based object location discrimination.

Mapping Cortical Regions Involved in Object Location Discrimination

We next used photoinhibition to survey the dorsal neocortex during specific epochs of the object location discrimination behavior ([Figure 1C](#)). We tested 55 evenly spaced cortical volumes for

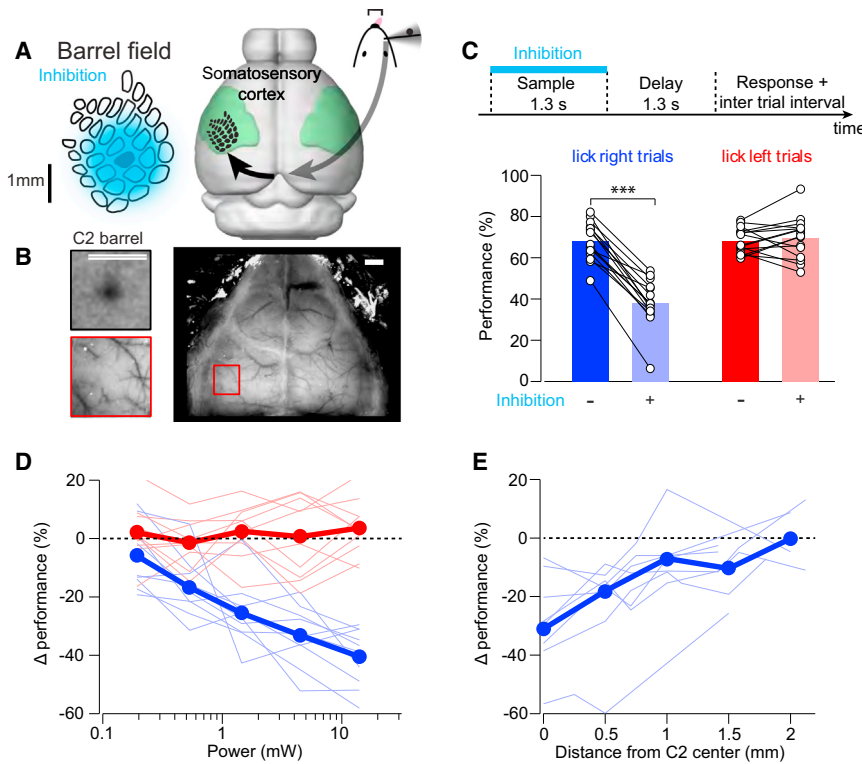


Figure 3. Photoinhibition of vS1 during Object Location Discrimination

(A) Approximate spatial extent of photoinhibition under our standard condition (1.5 mW). Photoinhibition spans at least ten barrel columns. Right: the primary somatosensory cortex (green), with the barrel field superposed.

(B) Mapping the C2 column with intrinsic signal imaging (top left) relative to vasculature landmarks (bottom left). Right: an example clear-skull cap. Scale bar, 1 mm.

(C) Photoinhibition of vS1 during the sample epoch. Top: timeline of photoinhibition. Bottom: effects of photoinhibition on behavior in “lick right” trials (blue) and “lick left” trials (red). Performance is the fraction of correct reports for each trial type (Experimental Procedures). Thin lines, individual mice (n = 15). Data from different laser powers are pooled (range, 0.97 to 14 mW; mean, 3.94 mW). ***p < 0.001, two-tailed t test.

(D) Change in performance caused by photoinhibition versus laser power. Blue, “lick right” trials; red, “lick left” trials. Thick lines, mean performance; thin lines, individual mice (n = 10).

(E) Change in performance in “lick right” trials versus photostimulus location from C2 barrel (n = 8). Laser power, 1.5 mW. See also Figure S5.

their involvement in the behavior (Figure 4A). We tested six mice across 151 behavioral sessions (53,190 trials). Photoinhibition was deployed in 75% of the trials at one of the 55 grid locations during either the sample or delay epochs (168 ± 11 “lick right” trials and 170 ± 11 “lick left” trials during sample epoch at each location; 150 ± 9 “lick right” trials and 150 ± 10 “lick left” trials during delay epoch at each location; mean \pm SD; see Experimental Procedures). We measured the mean performance change in “lick right” trials caused by photoinhibition at particular locations (Figure 4B, see Figure S6 for raw performance numbers).

Photoinhibition of most sites did not cause a detectable change in performance (Figures 4B and S6). During the sample epoch, photoinhibiting vS1 reduced performance (Figure 4B), consistent with the targeted vS1 experiments (Figure 3C). vS1 photoinhibition reduced performance significantly more during the sample epoch compared to the delay epoch ($p < 0.001$, two-tailed t test, Figure 4C), suggesting that tactile information dissipates rapidly in vS1 after the sample epoch. However, photoinhibition of vS1 during the delay period produced a small but significant effect ($p < 0.01$; two-tailed t test against 0; Figure 4C).

Photoinhibition during the delay epoch uncovered a frontal area (lateral ± 1.5 mm, bregma +2.5 mm) (Figures 4 and S6). This area was anterior and lateral to, and largely nonoverlapping with, the vibrissal primary motor cortex (vM1) (lateral 0.8 mm, bregma +1 mm) (Huber et al., 2012). At the spatial resolution of photoinhibition, this area was indistinguishable from the ALM area previously identified to play a role in high-level control of licking in mice (Komiyama et al., 2010) and rats (Travers et al.,

1997). We thus refer to this region as ALM. Photoinhibition of ALM on either side of the midline perturbed the animal’s performance, with the strongest effects during the delay epoch ($p \leq 0.05$, two-tailed t test, Figures 4D and 4E). Photoinhibition of the left ALM biased the choice toward the left lickport, resulting in an increased performance in “lick left” trials and decreased performance in “lick right” trials (Figure 4D). Photoinhibition of the right ALM biased the choice toward the right lickport (Figures 4E and S6). Unilateral photoinhibition of each side of ALM therefore yielded the opposite pattern of behavioral bias (Figures 4D and 4E). This suggests that unilateral photoinhibition of ALM biased the upcoming choice to the ipsilateral direction. We did not observe any effect of ALM photoinhibition on the animals’ licking latencies (sample epoch inhibition versus control trials, $p = 0.86$, paired t test, n = 6 mice; delay epoch versus control, $p = 0.48$, n = 6 mice).

Is ALM involved in motor preparation? We performed experiments in three new mice with the same pole locations but reversed motor choice (posterior \rightarrow lick left; anterior \rightarrow lick right) (Figures 5A and 5C). If a cortical area is involved in processing sensory information, the pattern of deficit caused by photoinhibition should be unchanged by this motor choice reversal. Indeed, the deficit caused by vS1 photoinhibition was similar as in the standard contingency, with a significant performance decrease in the “lick left” trials (Figure 5D). In contrast, if a cortical area is involved in determining the animal’s motor choice, the deficit caused by photoinhibition should be reversed. Consistent with this hypothesis, the bias in ALM photoinhibition was reversed by reversing the sensorimotor contingency (Figure 5D).

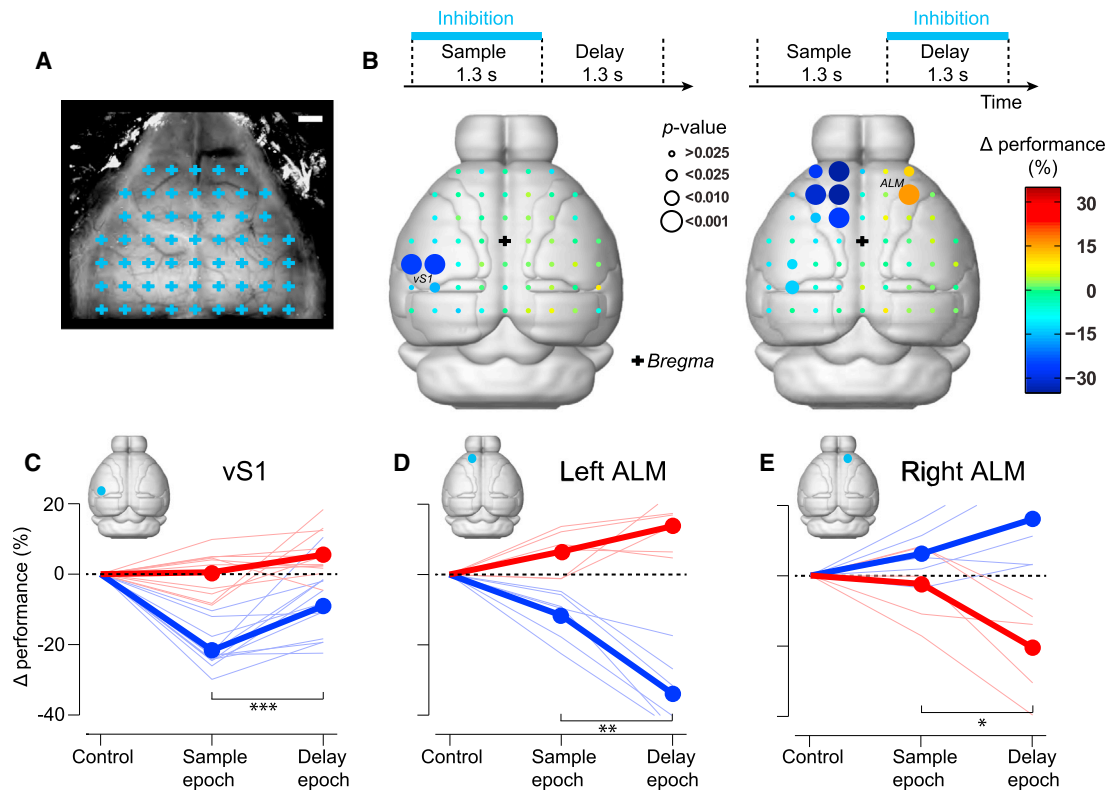


Figure 4. Cortical Areas Involved in Object Location Discrimination Revealed by Photoinhibition

(A) A grid of 55 photostimulus locations through the clear-skull cap (grid spacing, 1 mm). Each grid location was chosen randomly for photostimulation during either sample or delay epoch (see Experimental Procedures). Scale bar, 1 mm.

(B) Photoinhibition during different behavioral epochs. Top: photoinhibition during sample (left) and delay (right) epochs. Bottom: cortical regions involved in object location discrimination during sample (left) and delay (right) epochs in “lick right” trials. Color codes for the change in performance (%) under photoinhibition relative to control performance. Circle size codes for significance obtained from bootstrap (Experimental Procedures; from small to large; >0.025, <0.025, <0.01, <0.001). Effects on “lick left” trials are shown in Figure S6. Boundaries of cortical areas are from Allen Brain Atlas (Brain Explorer 2, <http://www.brain-map.org>).

(C) Photoinhibition of vS1 during the sample epoch caused a larger behavioral deficit than during the delay epoch in “lick right” trials (***, blue, “lick right” trials, $p < 0.001$, $n = 12$, two-tailed t test). Thick lines, mean; thin lines, individual mice.

(D) Photoinhibition of the left ALM during the delay epoch caused a larger behavioral deficit than during the sample epoch in “lick right” trials (**, blue, “lick right” trials, $p = 0.0016$, $n = 6$; two-tailed t test; red, “lick left” trials, $p = 0.09$).

(E) Photoinhibition of the right ALM during the delay epoch caused a larger behavioral deficit than during the sample epoch in “lick left” trials (blue, “lick right” trials, $p = 0.22$, $n = 5$; *, red, “lick left” trials, $p = 0.05$, two-tailed t test). See also Figure S6.

We validated the mapping experiments in two ways. First, we applied false discovery rate analyses to correct for multiple comparisons in our mapping results (Benjamini and Hochberg, 1995) (Experimental Procedures; Table S1). vS1 and ALM remained significant after the correction. Second, in a separate group of three mice, we targeted specific cortical regions (vS1, ALM, vM1, V1, and PPC; Figure S6). Only photoinhibition of vS1 and ALM produced significant behavioral changes (Figure S6). Even in experiments with bilateral photoinhibition of large areas overlapping PPC (simultaneous inhibition of eight grid points, Figure S6H), performance was not significantly affected.

We thus identified two cortical regions involved in tactile object location discrimination. Inactivation of vS1 during the sample epoch caused a deficit in pole detection regardless of motor choice. Unilateral inactivation of ALM during the delay epoch biased choice to the ipsilateral direction.

Neuronal Selectivity in vS1 and ALM

We recorded single units from vS1 and ALM in mice performing object location discrimination. A large fraction of vS1 neurons differentiated trial types (Figure 6B), typically with higher spike rates in “posterior” trials compared to “anterior” trials (Figure 6B). We computed “selectivity” as the difference in spike rates between the trial types (Figure 6C). The selectivity was largest at the beginning of the sample epoch (34/75 neurons significantly differentiated trial types in spike counts during the sample epoch, t test, $p < 0.05$), likely reflecting active touch (Figure 1D). Indeed, aligning the response to the first touch revealed a peak of activity with a 10 ms delay (Figure S7), consistent with previously reported latencies in vS1 (Armstrong-James et al., 1992; Brecht and Sakmann, 2002; O’Connor et al., 2013; Simons, 1978). Selectivity in vS1 was much reduced during the delay epoch (Figures 6C and 6D; selectivity sample versus

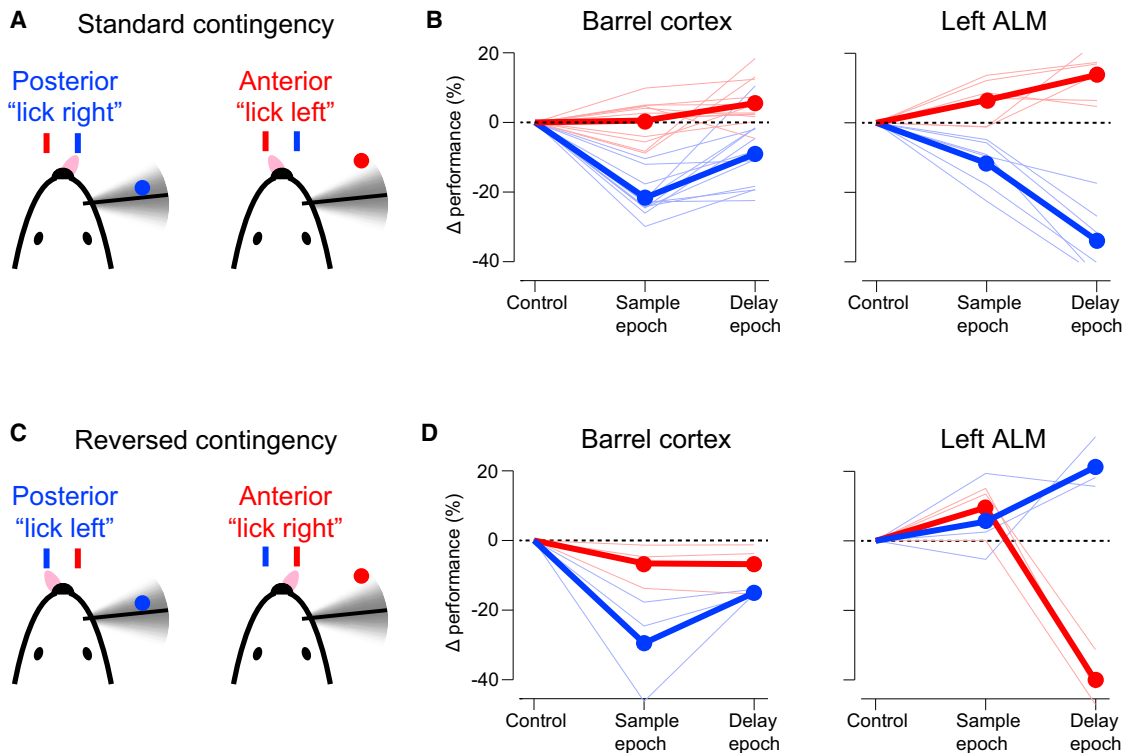


Figure 5. vS1 and ALM Contribute Differently to Behavior

- (A) “Lick left/lick right” task with standard contingency, in which mice learned to associate posterior pole position with licking right.
 (B) Photoinhibition of vS1 and left ALM during the sample and delay epochs; same as Figures 4C and 4D.
 (C) “Lick left/lick right” task with reversed contingency, in which mice learned to associate posterior pole position with licking left.
 (D) Photoinhibition of vS1 and left ALM during the sample and delay epochs under the reversed contingency.

delay: $p < 0.001$, paired t test); 20/75 neurons significantly differentiated trial types in spike counts during the delay epoch (t test, $p < 0.05$). Higher selectivity during the sample epoch compared to the delay epoch is consistent with the photoinhibition experiments (Figure 4C). The photoinhibition experiments also predicted that vS1 selectivity should be largely unaffected by the animals’ motor choice (Figure 5). Indeed, the selectivity was largely maintained on error trials (Figure 6E, slope = 0.47, $r = 0.54$, $p < 0.001$, also see examples in Figure 6B).

A large fraction of ALM neurons also differentiated between trial types (122/186; Figures 7A–7C). ALM selectivity emerged late in the sample epoch (13/186 neurons) and ramped up throughout the delay epoch (43/186 neurons), often long before the response (Figures 7B–7D; response type 1 and 2). Selectivity reached a maximum during the response epoch (99/186 neurons) (Figure 7E). In this respect, activity in ALM resembles preparatory activity previously seen in motor cortex in macaques (Tanji and Evarts, 1976). Immediately after the response cue, a subset of the neurons with preparatory activity became silent (23/186, response type 1, see example neuron in Figure 7B), whereas other neurons showed enhanced activity and selectivity (26/186, response type 2, Figure 7B). Another group of ALM neurons did not show preparatory activity but became active immediately after the response cue (63/186, response type 3, Figure 7B). This enhancement of selectivity immediately after

the response cue is consistent with a motor command (movement-related activity, Figure 7C response type 2 and 3). The preparatory and movement-related activity closely tracked the animals’ choice. In error trials, neurons switched their trial type preference (Figures 7F and 7G; delay epoch: slope = -0.41 , $r = -0.46$, $p < 0.001$; response epoch: slope = -0.48 , $r = -0.62$, $p < 0.001$; see examples in Figure 7B). This choice-specific selectivity is consistent with the ALM photoinhibition experiments (Figure 5).

In summary, neuronal selectivity in vS1 represents information about pole location independent of motor choice. Neuronal selectivity in ALM represents motor preparation and movement.

DISCUSSION

Cortical Information Flow during Tactile Decision Making

We developed a behavioral task for head-fixed mice that separated “sensation” and “action” in time (Figure 1). To map the cortical activity involved, we transiently and reversibly inactivated pyramidal neurons using photoinhibition in mice expressing ChR2 in GABAergic interneurons (Zhao et al., 2011). The photoinhibition was potent (Figure 2E), spatially restricted (Figure 2F), and temporally precise (Figure 2D). Head fixation, the

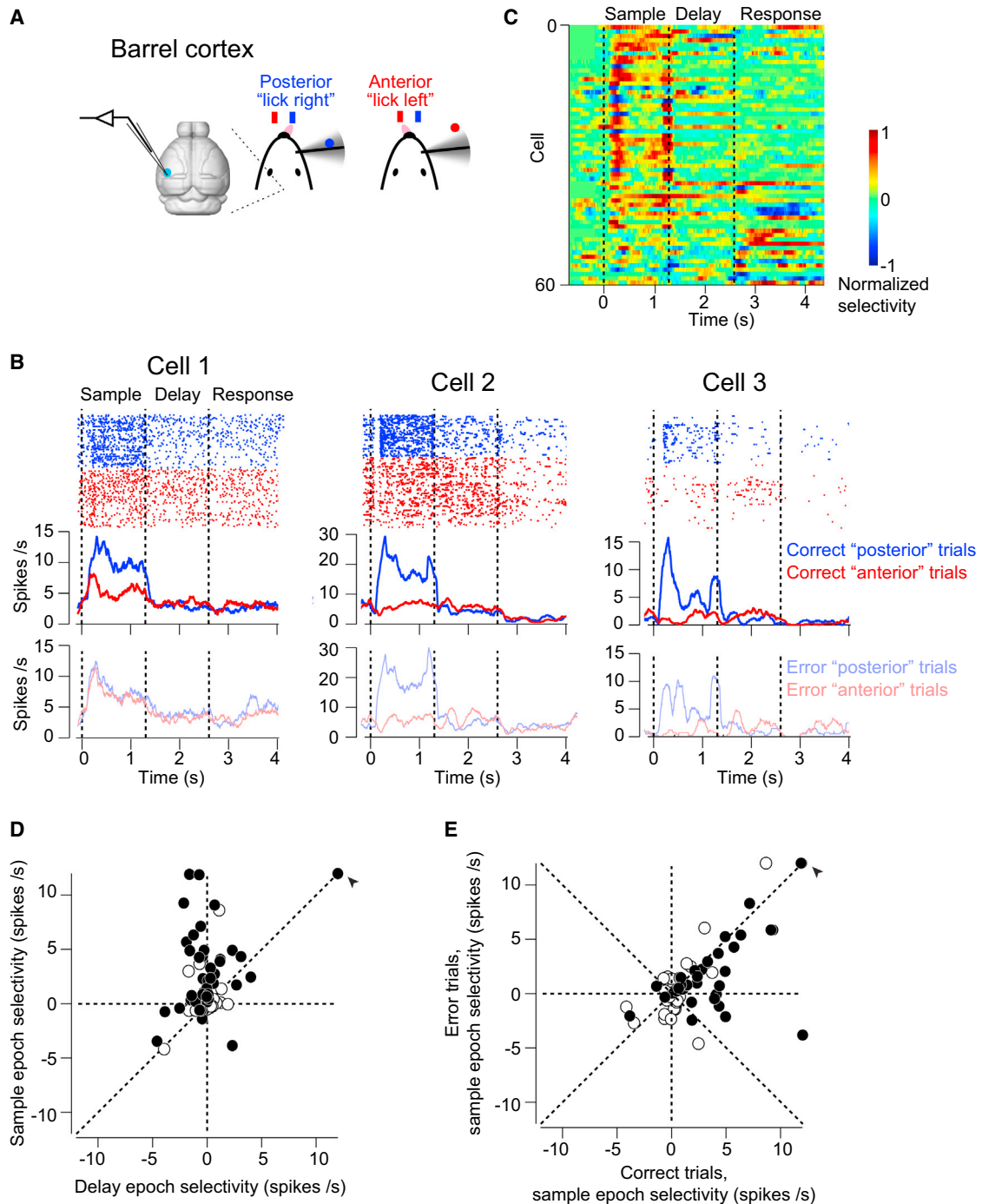


Figure 6. vS1 Neurons Show Stimulus-Specific Activity

(A) vS1 recording during behavior.
 (B) Three example vS1 neurons during object location discrimination. Top: spike raster and PSTH for correct "posterior" (blue) and "anterior" (red) trials. Bottom: PSTH for error trials (transparent color). Averaging window, 200 ms. Dashed lines delineate behavioral epochs.
 (C) vS1 population selectivity. Selectivity is the difference in spike rate between the "posterior" and "anterior" trials, normalized to the peak. Averaging window, 200 ms; 15/75 vS1 neurons did not show significant selectivity during any behavioral epoch, and they were excluded from the plot.
 (D) vS1 neurons are mainly selective during the sample epoch. Circles correspond to individual neurons ($n = 75$). Selectivity is the firing rate (FR) difference between "posterior" and "anterior" trials during sample or delay epoch ($FR_{\text{posterior}} - FR_{\text{anterior}}$). Filled circles indicate neurons with significant selectivity during either the sample or delay epoch ($p < 0.05$, two-tailed t test). Arrow, values are off scale; sample epoch selectivity, 19.4 spikes/s; delay epoch selectivity, 19 spikes/s.
 (E) vS1 maintains selectivity on error trials. Selectivity on correct trials versus error trials, slope = 0.47, $r = 0.54$, $p < 0.001$. Filled circles indicate neurons with significant sample epoch selectivity on the correct trials ($p < 0.05$, two-tailed t test). Arrow, the same outlier neuron as in (D). See also Figure S7.

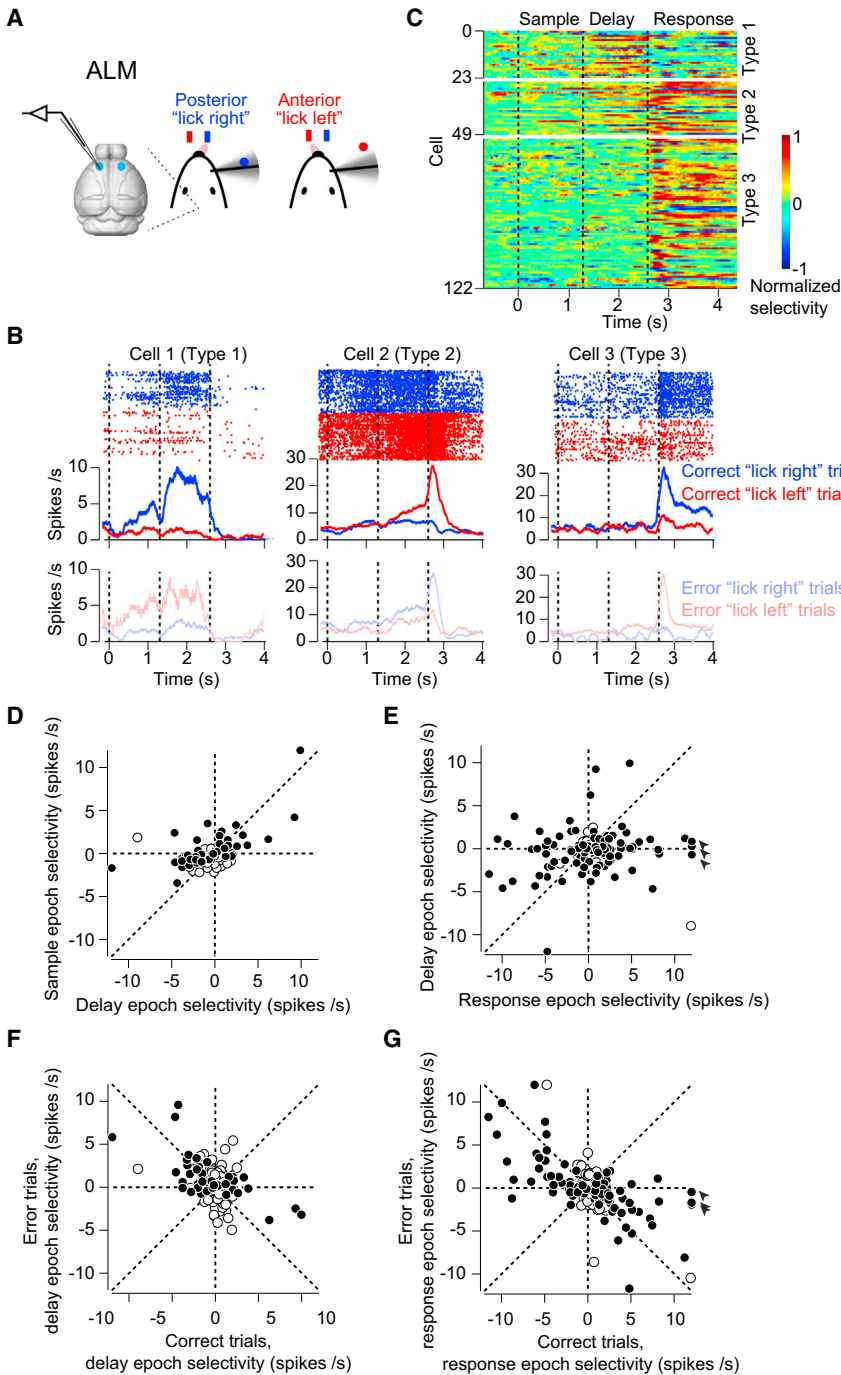


Figure 7. ALM Neurons Show Choice-Specific Preparatory and Movement-Related Activity

(A) ALM recording during behavior. (B) Three example ALM neurons during object location discrimination. Top: spike raster and PSTH for correct “lick right” (blue) and “lick left” (red) trials. Bottom: PSTH for error trials (transparent color). Averaging window, 200 ms. Dashed lines delineate behavioral epochs. (C) ALM population selectivity. Selectivity is the difference in spike rate between the preferred and nonpreferred trial type, normalized to the peak. For each neuron, we defined its preferred trial type (“lick right” or “lick left”) using spike counts from a subset of the trials (ten trials), and the remaining data were used to compute the selectivity. Averaging window, 200 ms. Six neurons of type 1 showed significant selectivity only during the sample epoch; thus, only 43 neurons showed significant delay epoch selectivity. (D) ALM neurons show choice-specific preparatory activity during the delay epoch. Selectivity is the firing rate (FR) difference between “lick right” and “lick left” trials during sample or delay epoch ($FR^{\text{lick right}} - FR^{\text{lick left}}$). Circles correspond to individual neurons ($n = 186$). Filled circles indicate neurons with significant selectivity during either the sample or delay epoch ($p < 0.05$, two-tailed t test). Data from both left ALM and right ALM are shown. (E) ALM neurons show movement-related selectivity during the response epoch. Circles correspond to individual neurons ($n = 186$). Filled circles indicate neurons with significant selectivity during either the delay or response epoch ($p < 0.05$, two-tailed t test). Arrows, values are off scale; response epoch selectivity, 12.5 spikes/s; 12.2 spikes/s, 16 spikes/s. (F) ALM preparatory activity during the delay epoch correlated with the animals’ behavioral choice. Selectivity on correct trials versus error trials, slope = -0.41 , $r = -0.46$, $p < 0.001$. Filled circles indicate neurons with significant delay epoch selectivity on the correct trials ($p < 0.05$, two-tailed t test). (G) ALM movement-related activity during the response epoch correlated with the animals’ behavioral choice. Selectivity on correct trials versus error trials, slope = -0.48 , $r = -0.62$, $p < 0.001$. Filled circles indicate neurons with significant response epoch selectivity on the correct trials ($p < 0.05$, two-tailed t test). Arrow, the same outlier neurons as in (E).

clear-skull cap preparation, and the laser-scanning system together provided access to most of the dorsal cortex for photo-inhibition (Figure 4A). We show that sensory processing in vS1 contributes to behavior mainly during the sample epoch, whereas a frontal region (ALM) is mainly required during the delay and early response epochs (Figure 4). Single-unit recordings supported these conclusions: a large fraction of neurons in vS1 show object location-dependent activity during the sample epoch (Figure 6), whereas the majority of neurons in

ALM are choice selective during the delay and response epochs (Figure 7).

Our study makes four contributions. First, we show that head-fixed mice can perform a symmetric-response perceptual decision behavior with a delay epoch. Translating perceptual decision behavioral paradigms to mice will facilitate understanding of the underlying neural circuit mechanisms. The delay epoch was critical, effectively boosting the time resolution of optogenetic inhibition. Individual mice performed many thousands of

trials with consistent performance. These features together allowed us to use focal photoinhibition to reveal the brain areas involved in specific task epochs.

Second, we outline a powerful method to inactivate small regions of cortex through the intact skull, by local photostimulation of Chr2-expressing GABAergic neurons. We characterized photoinhibition at unprecedented levels of detail (Figures 2 and S4). Photoinhibition allowed us to survey dozens of cortical regions (about half of the cortex) in individual mice. The scanning laser system also allows near-simultaneous photoinhibition of multiple cortical regions (Figure S6H; Experimental Procedures). The high throughput of this technique allows comprehensive surveys of multiple cortical regions underlying behaviors in mice.

Third, we identified two cortical regions involved in specific aspects of tactile decisions. vS1 is critical for the perception of object location (Figures 3, 5, and 6). Previous lesion and pharmacological inactivation studies of vS1 caused changes in motor strategies (Hutson and Masterton, 1986; O'Connor et al., 2010a), therefore the behavioral effect was confounded by motor deficits and possibly decreased levels of motivation (Kleinfeld and Deschênes, 2011). The motor strategies remained unchanged under transient photoinhibition (Figure S5), thus vS1 activity was critical for tactile sensation underlying object location discrimination. Lesion analysis of monkey somatosensation did not probe active sensation (Zainos et al., 1997). ALM is involved during the delay and response epochs (Figures 5 and 7), consistent with a role in motor preparation and movement.

Fourth, the photoinhibition and recording experiments outline the information flow underlying a tactile decision in the mouse cortex. Our data are consistent with a serial scheme, in which information is handed off from sensory to motor cortex, with little temporal overlap (Figures 6 and 7). Cortical information flow has previously been examined in primates using extracellular recording and correlations with behavior (de Lafuente and Romo, 2005; Hernández et al., 2010; Romo and de Lafuente, 2013), as well as electrical microstimulation (Bisley et al., 2001; de Lafuente and Romo, 2005; Seidemann et al., 1998). To our knowledge, ours is the first study to map task-relevant information flow on a cortex-wide scale using loss-of-function methods. It is possible that in more complex behavioral settings, or in difficult perceptual tasks, persistent reciprocal interactions may occur between sensory and motor areas. The neuronal selectivity in vS1 and ALM, and their contribution to behavior, provides hypotheses about neuronal coding and transformations between sensory and motor areas.

Relation to Previous Studies

Decision tasks with delay epochs have been widely used in nonhuman primates to study perception (Mountcastle et al., 1990; Seidemann et al., 1998), working memory (Fuster and Alexander, 1971; Goldman-Rakic, 1995; Romo et al., 1999), and motor preparation (Tanji and Evarts, 1976). The ability to separate behavioral events in time allowed for analyses and manipulations of specific behavioral components. Previously, Romo and colleagues have used a comparison task to separate tactile-flutter discrimination into sensation, working memory, and choice. Neuronal correlates of sensation, working memory,

and movement were found across a hierarchy of cortical areas (Hernández et al., 2010; Romo and de Lafuente, 2013). There is a surge of interest in developing similar behavioral tasks suitable for head-fixed mice (Harvey et al., 2012; Komiyama et al., 2010; O'Connor et al., 2010a; Pammer et al., 2013; Sanders and Kepecs, 2012). Our behavioral task design is similar to previous task designs in primates used to study how sensory information is evaluated for decision (de Lafuente and Romo, 2005; Seidemann et al., 1998); the key difference is that our mice were asked to actively move their whiskers for tactile sensation (O'Connor et al., 2010a, 2013; Pammer et al., 2013). The ability to carry out sophisticated behavioral tasks in mice opens up the possibility of investigating the circuits and cellular and synaptic mechanisms underlying perceptual decisions.

The involvement of vS1 in touch sensation (Figure 3) is consistent with previous studies (Hutson and Masterton, 1986; O'Connor et al., 2010a). Our data further show that vS1 is mainly involved during the sample epoch of the task. A partial deficit remained when vS1 was inactivated during the delay epoch, although this effect was small and heterogeneous across individual mice (Figure 4C). Consistently, our recording data from vS1 revealed that some cells signaled pole location throughout part of the delay epoch, after the pole was out of reach (Figure 6). Similarly, experiments in nonhuman primates showed that several visual areas contribute to visual decisions mainly during the sample epoch (Afraz et al., 2006; Bisley et al., 2001; Seidemann et al., 1998), with a small remaining effect during the delay epoch (Seidemann et al., 1998). A similar conclusion was inferred based on neuronal responses in somatosensory tasks (Hernández et al., 2010; Romo and de Lafuente, 2013).

Photoinhibition of vS1 in a similar task without a delay epoch leads to an increase in performance in the “anterior”/“lick left” trials (O'Connor et al., 2013). Addition of the delay epoch abolished this effect (Figure 4D). The underlying reasons for this difference are currently not understood. Photoinhibition during the sample epoch could produce some rebound activity during the delay epoch and thus increase the “lick right” rate (Figure 2D). Explaining this discrepancy will require an understanding of how vS1 activity is interpreted by downstream areas during the delay epoch.

The dissociation of vS1 activity and whisking (Figure S5) is likely not a general phenomenon but task specific. Previous studies have reported that perturbation of vS1 activity in other tasks can affect whisking (Matyas et al., 2010). The lack of vS1 involvement in whisking dovetails with an earlier lesion experiment in primate that showed that S1 lesions do not impair motor responses (Zainos et al., 1997).

Both the temporal specificity of photoinhibition (Figures 4D, 4E, and 5) and neuronal recording (Figure 7) support the idea that a dorsal anterior cortex (overlapping with “M2” in Paxinos and Franklin, 2004) is involved in motor preparation. Our results show that preparatory activity in the motor cortex (Tanji and Evarts, 1976) is causally related to action. This region overlaps with a previously reported motor area involved in control of licking (ALM, Komiyama et al., 2010; Travers et al., 1997) and we adopted this term here. The ALM defined here by photoinhibition (Figure 4B, center 1.5 mm lateral, 2.5 mm anterior to bregma) is slightly medial to the previously reported coordinates defined

by microstimulation (Komiyama et al., 2010, center, 2.0 mm lateral, 2.4 mm anterior) and extends into primary motor cortex (Figure 4B). The precise borders of ALM, if they exist, remain to be mapped.

Since the offset latency of photoinhibition was ~ 124 ms, ALM photoinhibition (Figure 4) cannot delineate between effects during delay epoch related to motor preparation and suppression of motor output during early parts of the response epoch. ALM neurons developed their selectivity gradually during the sample and delay epochs, reaching a maximum at the beginning of the response epoch (Figure 7). Ramping activity was also recently reported in rats performing a memory-guided orienting task (Erlich et al., 2011) in a region of the motor cortex that overlaps with the classical vibrissal motor cortex (vM1) (Brecht, 2011; Huber et al., 2012). Unilateral muscimol inactivation of this region biased the rats' choice in the ipsilateral direction. Our result is in broad agreement with this finding, in that unilateral inactivation of ALM biased licking in the ipsilateral direction (Figures 4D and 4E). This study also reported a mixture of neurons preferring either direction of orienting in each hemisphere (Erlich et al., 2011). Similarly, our recordings from ALM revealed a mixture of neurons preferring either direction of licking (Figure 7C). How these mixed, bilateral activity patterns are consistent with the lateralized inactivation behavioral effects (Figure 4) remains mysterious.

Inactivation of vM1 using muscimol causes behavioral deficits in mice trained in a "go/no-go" whisker-dependent object detection task (Huber et al., 2012). We did not observe consistent behavioral effects with vM1 inactivation in the "lick left/lick right" task (Figures 4B and S6). It is possible that differences in motor strategies could account for this discrepancy. In the "go/no-go" object detection task, poles were placed in one of multiple locations and the mouse was asked to report whether the pole was within reach or out of reach (Huber et al., 2012). Mice solved this task using large-amplitude, stereotyped whisking (peak to peak amplitude, $>40^\circ$), presumably to search for the pole. In contrast, in our experiments mice adapted a strategy with remarkably little rhythmic whisking (peak to peak amplitude, $<20^\circ$; Figure S5D).

Other Brain Areas in Tactile Decision Making

In the cortical mapping experiment we photoinhibited one cortical region at a time (Figure 4B). Several cortical areas could participate in tactile perception in parallel in a redundant manner. Inactivation of these areas simultaneously might be necessary to reveal their function.

Active perceptual decisions also involve subcortical regions, including the superior colliculus (Horwitz and Newsome, 1999), the striatum (Ding and Gold, 2010), and possibly the thalamus (Sommer and Wurtz, 2006). Targeting these subcortical regions, as well as the ventral cortex, for inactivation may require different methods of photoinhibition, for example using implantable optical fibers (Aravanis et al., 2007). Alternatively, red-shifted opsins (Lin et al., 2013; Packer et al., 2012) may allow noninvasive inactivation of deep brain structures.

Our survey of cortical areas involved in tactile decisions identified cortical regions at the beginning and the end of cortical processing. vS1 is the main conduit of tactile information from the

periphery to other cortical areas, including secondary somatosensory cortex (S2) and vM1 (Ferezou et al., 2007; Mao et al., 2011). vS1 also projects to thalamus and the dorsolateral striatum. ALM controls directional licking, the action indicating behavioral choice in our behavior. How does tactile information reach ALM? vS1 does not directly project to ALM (Mao et al., 2011), but at least three indirect pathways link vS1 and ALM. First, vS1 projects to S2, which projects to ALM (Allen Brain Institute for Brain Science, <http://mouse.brain-map.org>; Z.V.G., N.L., and K.S., unpublished data). An analogous pathway has been posited to play a key role in primate somatosensory decision tasks (Romo and de Lafuente, 2013). Second, vS1 projects to the posterior nucleus of the thalamus (PO), which projects to ALM. Third, vS1 projects to the dorsolateral striatum, which might shape decision-related activity in ALM via the output nuclei of the basal ganglia and motor thalamus. The specific roles of these different pathways will be the subject of future studies.

EXPERIMENTAL PROCEDURES

Animals and Surgical Procedures

This study is based on data from 38 mice (Table 1) (30 males; 8 females; 2 months to 10 months old). Nineteen *VGAT-ChR2-EYFP* mice (Jackson Laboratory, <http://www.jax.org>) were used for photoinhibition (Figures 3, 4, and 5) and neuronal recordings (Figures 6 and 7). Eight *VGAT-ChR2-EYFP* mice were used to characterize photoinhibition (Figure 2). Two *VGAT-ChR2-EYFP* mice were used for immunohistochemistry (Figure S2, not listed in Table 1). Two *VGAT-ChR2-EYFP* mice were used to characterize photoinhibition in striatum (Figure S2). Three wild-type mice (C57Bl/6Cr) were used for control behavioral testing (Figures S1E and S5). Four mice were used for measuring light transmission through the clear-skull cap (Figure S4; two *VGAT-ChR2-EYFP* mice and two transgenic mice in which *Rosa-LSL-H2B-GFP* mice, gift from Josh Huang, Cold Spring Harbor Laboratory, were crossed to *PV-IRES-Cre* mice; Hippenmeyer et al., 2005).

All procedures were in accordance with protocols approved by the Janella Farm Institutional Animal Care and Use Committee. Mice were implanted with a clear-skull cap constructed from a thin layer of clear dental cement over intact skull (Figure 3B) and a headpost. For silicon probe recording, a small craniotomy was made through the clear-skull cap. Neuronal recordings and photoinhibition in vS1 were guided by intrinsic signal imaging (Figure 3B) (Masino et al., 1993). Detailed information on water restriction and surgical procedures is provided in Supplemental Experimental Procedures.

Behavior

Mice were trained to perform object location discrimination through operant conditioning (O'Connor et al., 2010a; Supplemental Experimental Procedures). The hardware and software used for behavioral control was largely as described in O'Connor et al. (2010a) (see details in Supplemental Experimental Procedures). The stimulus was a pole (0.9 mm in diameter), presented at one of two possible positions (Figure 1). The two pole positions were 4.29 mm apart along the anterior-posterior axis (40° of whisking angle) and were constant across sessions. The posterior pole position was 5 mm from the whisker pad. A two-spout lickport (4.5 mm apart) was used to deliver water reward and record licks (Supplemental Experimental Procedures). Mouth movements (reaction time) were monitored using a photodiode and an infrared laser diode (Thorlabs). High-speed video was taken at 1 kHz using Mikrotron Eosens Camera (Norpix, MC1362) to track the C2 whisker (Supplemental Experimental Procedures).

At the beginning of each trial, the vertical pole moved into the plane within reach of the C2 whisker (0.2 s travel time). The sound produced by mechanically moving the pole triggered whisking before the pole was within reach (see Figure 1D example trial). The pole remained within reach for 1 s, after which it was retracted. The retraction time was 0.2 s, of which the pole

remained within reach in the first 0.1 s. Thus, we define the sample epoch as the time from onset of pole movement to 0.1 s after the retraction onset of the pole (sample epoch, 1.3 s total; [Figure 1C](#)). The delay epoch lasted for another 1.2 s after the completion of pole retraction (delay epoch, 1.3 s total; [Figure 1C](#)). An auditory “response” cue indicated the end of the delay epoch (pure tone, 3.4 kHz, 0.1 s duration, DigiKey, 458-1088-ND). Licking early during the trial was punished by a loud “alarm” sound (siren buzzer, 0.05 s duration, RadioShack, 273-079), followed by a brief timeout (1–1.2 s). Continued licking triggered additional timeouts; these trials were excluded from the analyses (“lick early” trials; [Figure 1E](#), black bars). Licking the correct lickport after the auditory “response” cue led to a small drop of liquid reward (3 μ l). Licking the incorrect lickport triggered a timeout (2–5 s). Trials in which mice did not lick within a 1.5 s window after the “response” cue were rare and typically occurred at the end of a session. Sessions were terminated when signs of fatigue were observed (e.g., reduced whisking, occurrence of “no lick” trials). Typically, the last 20 trials within each session were excluded from analyses. All mice learned to perform this task with the C2 whisker. The total training time to criterion performance (>70% correct) was 3–4 weeks ([Figure S1](#)) (see details in [Supplemental Experimental Procedures](#)).

Photostimulation

Light from a 473 nm laser (DHOM-M-473-200, UltraLaser) was controlled by an acousto-optical modulator (AOM; MTS110-A3-VIS, Quanta Tech) and a shutter (Vincent Associates), coupled to a 2D scanning galvo system (GVSM002, Thorlabs), then focused onto the brain surface ([Figure 1A](#); [Supplemental Experimental Procedures](#)). The laser at the brain surface had a Gaussian profile with a beam diameter of 400 μ m at 4σ ([Figure S4](#)). The scanning galvo system (0.5–5 ms step time for step size 0.57–35 mm) and AOM (extinction ratio 1:2,000; 1 μ s rise time) allowed simultaneous targeting of multiple nonadjacent cortical regions for photostimulation ([Figure S6H](#)).

The standard photostimulus had a near sinusoidal temporal profile (40 Hz) with a linear attenuation in intensity over the last 100 ms (duration: 1.3 s + 0.1 s ramp, [Figure 2D](#)). The power values reported is the time average. To prevent the mice from distinguishing photostimulation trials from control trials using visual cues, we delivered a “masking flash” (40, 1 ms pulses at 10 Hz) using a blue LED near the eyes ([Supplemental Experimental Procedures](#)). The masking flash began as the pole started to move and continued through the end of the epoch in which photostimulation could occur.

For photostimulation of vS1, the laser beam was positioned over the C2 barrel column. For photostimulation of multiple cortical locations ([Figure 4](#)), the laser beam was aligned to bregma. For sessions in which we targeted specific cortical regions, photostimulation was delivered on 25% of behavioral trials. Photostimulation locations were chosen randomly but never twice in succession. For sessions in which we targeted 55 cortical locations ([Figures 4B and S6](#)), photostimulation was delivered on 75% of behavioral trials. Each cortical location was photostimulated once in random order over 55 stimulation trials.

For recording in awake nonbehaving mice, photostimulation was delivered at \sim 7 s intervals (data in [Figure 2](#)). The power (0.53, 1.0, 1.5, 2.5, 4.5, 7.3, and 14 mW) and locations of photostimulation (0.5, 0.75, 1.0, 2.0, and 3.0 mm from the recording sites) were chosen randomly. In addition to vS1 ([Figure 2](#)), we tested photoinhibition in ALM during behavior and found identical effects ([Figure S4I](#)). Furthermore, photoinhibition was similar during the sample and delay epochs ([Figure S4I](#)).

We measured light transmission through the clear-skull cap (dental cement and skull) using two independent methods. First, we directly measured laser power before and after passing through the isolated clear-skull cap ([Figure S4F](#)). Second, we measured the rate of photobleaching in vivo in a transgenic mouse line expressing GFP in the nuclei of a subset of neurons (*Rosa-LSL-H2B-GFP*, crossed to *PV-IRES-Cre*). Photobleaching was induced by prolonged (10 min) illumination at different laser powers with and without the clear-skull cap. Nuclear fluorescence was measured in fixed tissue sections ([Figure S4](#)). Both methods gave light transmission of approximately 50%.

Neuronal Recordings

Extracellular spikes were recorded using silicon probes (NeuroNexus) (for details see [Supplemental Experimental Procedures](#)). Under awake, nonbehaving condition, mice remained idle while different photostimulation conditions were

tested. For recordings during behavior, sessions started after setting up the recording apparatus. At the end of the recording sessions, the electrode was removed and the craniotomy was covered with Kwik-Sil (World Precision Instruments) and further reinforced with dental acrylic. On subsequent days, recordings were made through the same craniotomy. Due to deterioration of the neuronal tissue caused by electrode penetrations, only one to three recordings were made in each craniotomy. In a subset of mice, two craniotomies were made for recording from vS1 and ALM ([Table 1](#)). Silicon probes were painted with Dil and recording tracks were recovered to measure recording depth.

Data Analysis

We separately computed the performance for “lick right” and “lick left” trials as the fraction of correct reports ([Figures 1E and 3C](#)). Chance performance was 50%. Behavioral effects of photoinhibition were quantified by comparing the performance under photostimulation with control performance ([Figures 3 and 4](#)). Significance was determined using two-tailed t test ([Figures 1, 3, 4C–4E, 6, and 7](#)) and bootstrap ([Figure 4B](#)).

We tested against the null hypothesis that each photoinhibition site did not cause a performance change. Performance changes must be interpreted against behavioral variability. We performed bootstrap to consider the variability across mice, sessions, and trials ([Efron and Tibshirani, 1994](#)). For each cycle of bootstrap, repeated 10^6 times, we randomly sampled with replacement (1) animals, (2) sessions performed by each animal, and (3) trials within each session. We computed control performance and performance under photoinhibition for each condition (i.e., “lick right” and “lick left” trial performances for each cortical location). The p value for each photoinhibition condition was the fraction of times the performance change from the control condition changed sign (if photoinhibition showed a mean decrease in performance from the control, p value for this condition was the number of times it showed an increase in performance during bootstrap). This p value can be interpreted as follows: if we were to repeat this experiment, what is the chance that we would not see the performance change observed here? The bootstrap analysis determined the confidence interval around our originally observed performance values (the SEs of performance were the SDs of the estimates from bootstrap; these were reported as error bars in [Figure S6](#)), and the duality of confidence intervals and hypotheses testing allowed us to report that confidence interval as a p value ([Efron and Tibshirani, 1994](#)). The threshold p value was $\alpha = 0.025$ (for one-tailed tests). To correct for multiple comparisons, we used the Benjamini-Hochberg procedure ([Benjamini and Hochberg, 1995](#)): we first sorted the p values corresponding to the 55 photoinhibition locations in ascending order (i.e., $p(1) \leq p(2) \leq \dots \leq p(i) \leq \dots \leq p(55)$) and found the largest i such that $p(i) \leq \alpha \cdot i/55$. The performance change for grid locations, 1, \dots , i , was scored as significant ([Table S1](#)). We performed power analyses to estimate the number of trials necessary to observe significant performance changes under normal behavioral variability. We randomly down sampled the full data set (53,190 behavioral trials) and recomputed p values to look for the minimal sample size needed to reach $p < 0.025$. The minimal sample size depended on the mean effect size. For ALM, (mean Δ performance, 26%, [Figure 4B](#), “lick right” trials, delay epoch), a minimal of 75 photoinhibition trials were needed to observe a significant performance change (156 trials were collected). For vS1, (mean Δ performance, 23%, [Figure 4B](#), “lick right” trials, sample epoch), a minimal of 91 photoinhibition trials were needed to observe a significant performance change (174 trials were collected). With the full data set (53,190 behavioral trials), we could reliably detect a minimal behavioral change of 10% ([Figure 4B](#)).

The extracellular recording traces were band-pass filtered (300–6,000 Hz). Events that exceeded an amplitude threshold (four SDs of the background) were subjected to manual spike sorting to extract single units (see details in [Supplemental Experimental Procedures](#)). We recorded 133 single units under awake, nonbehaving conditions ([Table 1](#)). For each unit, its spike width was computed as the trough to peak interval in the mean spike waveform ([Figures 2C and S3](#)). We defined units with spike width <0.35 ms as FS neurons (18/133) and units with spike width >0.45 ms as putative pyramidal neurons (ppy, 106/133). Units with intermediate values (0.35–0.45 ms, 9/133) were excluded from our analyses.

Effect of photoinhibition on activity was quantified in “normalized spike rate” relative to the baseline (see [Supplemental Experimental Procedures](#)). The time

course of photoinhibition (onset, 17.3 ± 1.4 ms, mean \pm SEM; offset 124 ± 9.4 ms) was computed from averaged PSTH (Figure 2D; see Supplemental Experimental Procedures). Bootstrap was performed over neurons to obtain the standard errors.

Under the active behaving condition, 261 neurons were isolated for >40 behavioral trials (>20 “lick right” trials and >20 “lick left” trials). We recorded 75 neurons from vS1 and 138 neurons were recorded from the left ALM and 48 neurons were recorded from the right ALM. These neurons were further screened for significant trial-type selectivity using spike count during the sample, delay, or response epoch (two-tailed t test, Figures 6 and 7, filled symbols). For this analysis, only trials in which the mice correctly reported pole locations were included. To quantify the effect of photoinhibition during active behavior, we focused our analysis on 35/75 vS1 neurons (six mice) that were classified as pyramidal neurons and tested for >5 photostimulation trials (25% of the trials). These neurons were presented in Figure 2E. A few recording sessions were discarded due to excessive bleeding (7/25 sessions) over the craniotomy.

SUPPLEMENTAL INFORMATION

Supplemental Information includes Supplemental Experimental Procedures, seven figures, and one table and can be found with this article online at <http://dx.doi.org/10.1016/j.neuron.2013.10.020>.

AUTHOR CONTRIBUTIONS

Z.V.G., N.L., and K.S. conceived the project. Z.V.G. and N.L. performed the experiments. Z.V.G., N.L., and E.O. performed animal training. Z.V.G., N.L., and K.S. analyzed the data. D.H. developed the clear-skull cap preparation and performed pilot studies using the “lick left/lick right” task. D.G. developed the silicon probe recording system and the lickport system. J.T.T. and G.F. provided the *VGAT-ChR2-EYFP* transgenic mice. Z.V.G., N.L., and K.S. wrote the paper with comments from other authors.

ACKNOWLEDGMENTS

We thank Carlos Brody, Daniel O'Connor, Misha Ahrens, Mac Hooks, Nick Sofroniew, Jianing Yu, Tsai-Wen Chen, Simon Peron, and Dima Rinberg for comments on the manuscript, Susan Michael and Amy Hu for histology, S. Andrew Hires for help with whisker tracking, Daniel O'Connor for help with the laser-scanning system, and Tim Harris, Brian Barbarits, and Anthony Leonardo for help with silicon probe recordings. This work was funded by Howard Hughes Medical Institute. N.L. is a Helen Hay Whitney Foundation postdoctoral fellow.

Accepted: October 2, 2013

Published: December 19, 2013

REFERENCES

- Afraz, S.R., Kiani, R., and Esteky, H. (2006). Microstimulation of inferotemporal cortex influences face categorization. *Nature* 442, 692–695.
- Aravanis, A.M., Wang, L.P., Zhang, F., Meltzer, L.A., Mogri, M.Z., Schneider, M.B., and Deisseroth, K. (2007). An optical neural interface: in vivo control of rodent motor cortex with integrated fiberoptic and optogenetic technology. *J. Neural Eng.* 4, S143–S156.
- Armstrong-James, M., Fox, K., and Das-Gupta, A. (1992). Flow of excitation within rat barrel cortex on striking a single vibrissa. *J. Neurophysiol.* 68, 1345–1358.
- Benjamini, Y., and Hochberg, Y. (1995). Controlling the false discovery rate: a practical and powerful approach to multiple testing. *J. R. Stat. Soc. B* 57, 289–300.
- Bisley, J.W., Zaksas, D., and Pasternak, T. (2001). Microstimulation of cortical area MT affects performance on a visual working memory task. *J. Neurophysiol.* 85, 187–196.
- Brecht, M. (2011). Movement, confusion, and orienting in frontal cortices. *Neuron* 72, 193–196.
- Brecht, M., and Sakmann, B. (2002). Dynamic representation of whisker deflection by synaptic potentials in spiny stellate and pyramidal cells in the barrels and septa of layer 4 rat somatosensory cortex. *J. Physiol.* 543, 49–70.
- Clack, N.G., O'Connor, D.H., Huber, D., Petreanu, L., Hires, A., Peron, S., Svoboda, K., and Myers, E.W. (2012). Automated tracking of whiskers in videos of head fixed rodents. *PLoS Comput. Biol.* 8, e1002591.
- Curtis, J.C., and Kleinfeld, D. (2009). Phase-to-rate transformations encode touch in cortical neurons of a scanning sensorimotor system. *Nat. Neurosci.* 12, 492–501.
- de Lafuente, V., and Romo, R. (2005). Neuronal correlates of subjective sensory experience. *Nat. Neurosci.* 8, 1698–1703.
- Ding, L., and Gold, J.I. (2010). Caudate encodes multiple computations for perceptual decisions. *J. Neurosci.* 30, 15747–15759.
- Efron, B., and Tibshirani, R. (1994). *An Introduction to the Bootstrap*, First Edition. (Boca Raton: Chapman and Hall/CRC).
- Erich, J.C., Bialek, M., and Brody, C.D. (2011). A cortical substrate for memory-guided orienting in the rat. *Neuron* 72, 330–343.
- Felleman, D.J., and Van Essen, D.C. (1991). Distributed hierarchical processing in the primate cerebral cortex. *Cereb. Cortex* 1, 1–47.
- Ferezou, I., Haiss, F., Gentet, L.J., Aronoff, R., Weber, B., and Petersen, C.C. (2007). Spatiotemporal dynamics of cortical sensorimotor integration in behaving mice. *Neuron* 56, 907–923.
- Fuster, J.M., and Alexander, G.E. (1971). Neuron activity related to short-term memory. *Science* 173, 652–654.
- Gold, J.I., and Shadlen, M.N. (2002). Banburismus and the brain: decoding the relationship between sensory stimuli, decisions, and reward. *Neuron* 36, 299–308.
- Goldman-Rakic, P.S. (1995). Cellular basis of working memory. *Neuron* 14, 477–485.
- Harvey, C.D., Coen, P., and Tank, D.W. (2012). Choice-specific sequences in parietal cortex during a virtual-navigation decision task. *Nature* 484, 62–68.
- Helmstaedter, M., Sakmann, B., and Feldmeyer, D. (2009). L2/3 interneuron groups defined by multiparameter analysis of axonal projection, dendritic geometry, and electrical excitability. *Cereb. Cortex* 19, 951–962.
- Hernández, A., Nácher, V., Luna, R., Zainos, A., Lemus, L., Alvarez, M., Vázquez, Y., Camarillo, L., and Romo, R. (2010). Decoding a perceptual decision process across cortex. *Neuron* 66, 300–314.
- Hikosaka, O., and Wurtz, R.H. (1985). Modification of saccadic eye movements by GABA-related substances. I. Effect of muscimol and bicuculline in monkey superior colliculus. *J. Neurophysiol.* 53, 266–291.
- Hippenmeyer, S., Vrieseling, E., Sigrist, M., Portmann, T., Laengle, C., Ladle, D.R., and Arber, S. (2005). A developmental switch in the response of DRG neurons to ETS transcription factor signaling. *PLoS Biol.* 3, e159.
- Hoffer, Z.S., Arantes, H.B., Roth, R.L., and Alloway, K.D. (2005). Functional circuits mediating sensorimotor integration: quantitative comparisons of projections from rodent barrel cortex to primary motor cortex, neostriatum, superior colliculus, and the pons. *J. Comp. Neurol.* 488, 82–100.
- Hooks, B.M., Mao, T., Gutnisky, D.A., Yamawaki, N., Svoboda, K., and Shepherd, G.M. (2013). Organization of cortical and thalamic input to pyramidal neurons in mouse motor cortex. *J. Neurosci.* 33, 748–760.
- Horwitz, G.D., and Newsome, W.T. (1999). Separate signals for target selection and movement specification in the superior colliculus. *Science* 284, 1158–1161.
- Huber, D., Gutnisky, D.A., Peron, S., O'Connor, D.H., Wiegert, J.S., Tian, L., Oertner, T.G., Looger, L.L., and Svoboda, K. (2012). Multiple dynamic representations in the motor cortex during sensorimotor learning. *Nature* 484, 473–478.
- Hutson, K.A., and Masterton, R.B. (1986). The sensory contribution of a single vibrissa's cortical barrel. *J. Neurophysiol.* 56, 1196–1223.

- Kawaguchi, Y. (1993). Groupings of nonpyramidal and pyramidal cells with specific physiological and morphological characteristics in rat frontal cortex. *J. Neurophysiol.* *69*, 416–431.
- Kleinfeld, D., and Deschênes, M. (2011). Neuronal basis for object location in the vibrissa scanning sensorimotor system. *Neuron* *72*, 455–468.
- Knutsen, P.M., Pietr, M., and Ahissar, E. (2006). Haptic object localization in the vibrissal system: behavior and performance. *J. Neurosci.* *26*, 8451–8464.
- Komiyama, T., Sato, T.R., O'Connor, D.H., Zhang, Y.X., Huber, D., Hooks, B.M., Gabbito, M., and Svoboda, K. (2010). Learning-related fine-scale specificity imaged in motor cortex circuits of behaving mice. *Nature* *464*, 1182–1186.
- Koralek, K.A., Jensen, K.F., and Killackey, H.P. (1988). Evidence for two complementary patterns of thalamic input to the rat somatosensory cortex. *Brain Res.* *463*, 346–351.
- Lin, J.Y., Knutsen, P.M., Muller, A., Kleinfeld, D., and Tsien, R.Y. (2013). ReaChR: a red-shifted variant of channelrhodopsin enables deep transcranial optogenetic excitation. *Nat. Neurosci.* *16*, 1499–1508.
- Long, M.A., and Fee, M.S. (2008). Using temperature to analyse temporal dynamics in the songbird motor pathway. *Nature* *456*, 189–194.
- Lu, S.M., and Lin, R.C.S. (1993). Thalamic afferents of the rat barrel cortex: a light- and electron-microscopic study using *Phaseolus vulgaris* leucoagglutinin as an anterograde tracer. *Somatosens. Mot. Res.* *10*, 1–16.
- Luo, L., Callaway, E.M., and Svoboda, K. (2008). Genetic dissection of neural circuits. *Neuron* *57*, 634–660.
- Mao, T., Kusefoglou, D., Hooks, B.M., Huber, D., Petreanu, L., and Svoboda, K. (2011). Long-range neuronal circuits underlying the interaction between sensory and motor cortex. *Neuron* *72*, 111–123.
- Masino, S.A., Kwon, M.C., Dory, Y., and Frostig, R.D. (1993). Characterization of functional organization within rat barrel cortex using intrinsic signal optical imaging through a thinned skull. *Proc. Natl. Acad. Sci. USA* *90*, 9998–10002.
- Matyas, F., Sreenivasan, V., Marbach, F., Wacongne, C., Barsy, B., Mateo, C., Aronoff, R., and Petersen, C.C. (2010). Motor control by sensory cortex. *Science* *330*, 1240–1243.
- McCormick, D.A., Connors, B.W., Lighthall, J.W., and Prince, D.A. (1985). Comparative electrophysiology of pyramidal and sparsely spiny stellate neurons of the neocortex. *J. Neurophysiol.* *54*, 782–806.
- Mountcastle, V.B., Steinmetz, M.A., and Romo, R. (1990). Frequency discrimination in the sense of flutter: psychophysical measurements correlated with postcentral events in behaving monkeys. *J. Neurosci.* *10*, 3032–3044.
- O'Connor, D.H., Huber, D., and Svoboda, K. (2009). Reverse engineering the mouse brain. *Nature* *461*, 923–929.
- O'Connor, D.H., Clack, N.G., Huber, D., Komiyama, T., Myers, E.W., and Svoboda, K. (2010a). Vibrissa-based object localization in head-fixed mice. *J. Neurosci.* *30*, 1947–1967.
- O'Connor, D.H., Peron, S.P., Huber, D., and Svoboda, K. (2010b). Neural activity in barrel cortex underlying vibrissa-based object localization in mice. *Neuron* *67*, 1048–1061.
- O'Connor, D.H., Hires, S.A., Guo, Z.V., Li, N., Yu, J., Sun, Q.Q., Huber, D., and Svoboda, K. (2013). Neural coding during active somatosensation revealed using illusory touch. *Nat. Neurosci.* *16*, 958–965.
- Packer, A.M., Peterka, D.S., Hirtz, J.J., Prakash, R., Deisseroth, K., and Yuste, R. (2012). Two-photon optogenetics of dendritic spines and neural circuits. *Nat. Methods* *9*, 1202–1205.
- Pammer, L., O'Connor, D.H., Hires, S.A., Clack, N.G., Huber, D., Myers, E.W., and Svoboda, K. (2013). The mechanical variables underlying object localization along the axis of the whisker. *J. Neurosci.* *33*, 6726–6741.
- Paxinos, G., and Franklin, H.B.J. (2004). *The Mouse Brain in Stereotaxic Coordinates: Compact, Second Edition.* (Amsterdam: Elsevier).
- Petreanu, L., Mao, T., Sternson, S.M., and Svoboda, K. (2009). The subcellular organization of neocortical excitatory connections. *Nature* *457*, 1142–1145.
- Ponce, C.R., Lomber, S.G., and Born, R.T. (2008). Integrating motion and depth via parallel pathways. *Nat. Neurosci.* *11*, 216–223.
- Ritt, J.T., Andermann, M.L., and Moore, C.I. (2008). Embodied information processing: vibrissa mechanics and texture features shape micromotions in actively sensing rats. *Neuron* *57*, 599–613.
- Romo, R., and de Lafuente, V. (2013). Conversion of sensory signals into perceptual decisions. *Prog. Neurobiol.* *103*, 41–75.
- Romo, R., Brody, C.D., Hernández, A., and Lemus, L. (1999). Neuronal correlates of parametric working memory in the prefrontal cortex. *Nature* *399*, 470–473.
- Sanders, J.I., and Kepecs, A. (2012). Choice ball: a response interface for two-choice psychometric discrimination in head-fixed mice. *J. Neurophysiol.* *108*, 3416–3423.
- Schwarz, C., Hentschke, H., Butovas, S., Haiss, F., Stüttgen, M.C., Gerdjikov, T.V., Bergner, C.G., and Waiblinger, C. (2010). The head-fixed behaving rat—procedures and pitfalls. *Somatosens. Mot. Res.* *27*, 131–148.
- Seidemann, E., Zohary, E., and Newsome, W.T. (1998). Temporal gating of neural signals during performance of a visual discrimination task. *Nature* *394*, 72–75.
- Simons, D.J. (1978). Response properties of vibrissa units in rat SI somatosensory neocortex. *J. Neurophysiol.* *41*, 798–820.
- Sommer, M.A., and Wurtz, R.H. (2006). Influence of the thalamus on spatial visual processing in frontal cortex. *Nature* *444*, 374–377.
- Tanji, J., and Evarts, E.V. (1976). Anticipatory activity of motor cortex neurons in relation to direction of an intended movement. *J. Neurophysiol.* *39*, 1062–1068.
- Travers, J.B., Dinardo, L.A., and Karimnamazi, H. (1997). Motor and premotor mechanisms of licking. *Neurosci. Biobehav. Rev.* *21*, 631–647.
- Voigts, J., Sakmann, B., and Celikel, T. (2008). Unsupervised whisker tracking in unrestrained behaving animals. *J. Neurophysiol.* *100*, 504–515.
- von Heimendahl, M., Itskov, P.M., Arabzadeh, E., and Diamond, M.E. (2007). Neuronal activity in rat barrel cortex underlying texture discrimination. *PLoS Biol.* *5*, e305.
- Woolsey, T.A., and Van der Loos, H. (1970). The structural organization of layer IV in the somatosensory region (SI) of mouse cerebral cortex. The description of a cortical field composed of discrete cytoarchitectonic units. *Brain Res.* *17*, 205–242.
- Zainos, A., Merchant, H., Hernández, A., Salinas, E., and Romo, R. (1997). Role of primary somatic sensory cortex in the categorization of tactile stimuli: effects of lesions. *Exp. Brain Res.* *115*, 357–360.
- Zhao, S., Ting, J.T., Atallah, H.E., Qiu, L., Tan, J., Gloss, B., Augustine, G.J., Deisseroth, K., Luo, M., Graybiel, A.M., and Feng, G. (2011). Cell type-specific channelrhodopsin-2 transgenic mice for optogenetic dissection of neural circuitry function. *Nat. Methods* *8*, 745–752.